

P. O'SHEA*,
 S. AKTURK
 M. KIMMEL
 R. TREBINO

Practical issues in ultra-short-pulse measurements with 'GRENOUILLE'

School of Physics, Georgia Institute of Technology, Atlanta, GA 30332-0430, USA

Received: 25 May 2004/Revised version: 26 July 2004
 Published online: 29 September 2004 • © Springer-Verlag 2004

ABSTRACT We examine the characteristics and limitations of GRENOUILLE, a simple and compact implementation of the second-harmonic-generation (SHG) frequency-resolved-optical-gating (FROG) technique. We show that it can be made to operate effectively over a relatively wide range of pulse lengths and wavelengths. We also describe procedures for its design and calibration, and we discuss the use of arbitrary non-linear SHG crystals.

PACS 42.65.-k; 42.65.Re

1 Introduction

The introduction of frequency-resolved optical gating (FROG) [1] a little over a decade ago made the measurement of the complete time-dependent intensity and phase of ultra-short laser pulses possible [2], as well as sensitive [3], reliable [4], and accurate [5]. With the recent introduction of grating-eliminated no-nonsense observation of ultra-fast laser-light E-fields (GRENOUILLE) [6], a variant of second-harmonic-generation (SHG) FROG, which has no sensitive alignment parameters, FROG has also become extremely simple, inexpensive, compact, and easy to use. It also yields a wealth of additional information. With most implementations of GRENOUILLE, it is straightforward to also measure the beam spatial profile, and GRENOUILLE (see Figs. 1 and 2) has recently been shown to also measure accurately the important spatio-temporal distortions, spatial chirp [7], and pulse-front tilt [8], without modification to its apparatus.

GRENOUILLE has several advantages over other ultra-short-pulse measurement techniques, including its close relatives in the FROG family. Most notably, its use of a thick SHG crystal, which simultaneously performs the required autocorrelation and provides the required spectral resolution, eliminates the bulky spectrometer and significantly increases the device sensitivity. In addition, the Fresnel biprism, which replaces the beam splitter, translation stage, and beam-

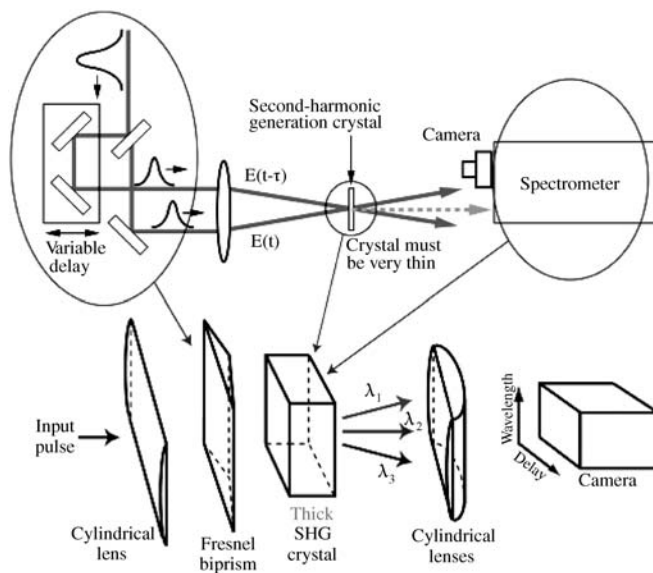


FIGURE 1 An SHG FROG device (above) and the simpler version, GRENOUILLE (below)

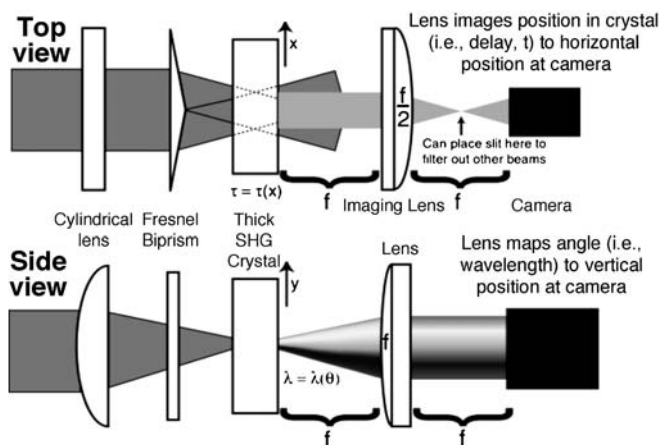


FIGURE 2 Top and side views of GRENOUILLE device

combining optics, simplifies its setting up tremendously and eliminates the need for re-alignment over time.

However, these choices are not without trade-offs: for instance, the thick SHG crystal used to spectrally resolve the signal has less spectral resolution than the spectrometer used

* Fax: +1-703-704-1753, E-mail: poshea@nvl.army.mil
 * Current address: US Army Night Vision and Electronic Sensors Directorate, Fort Belvoir, VA 22060-5806, USA

in a standard SHG FROG device. Also, the thick crystal has group-velocity dispersion (GVD), which could unacceptably distort a very short pulse. Thus, to make the most of GRENOUILLE and to know when to use it over a more standard FROG device, it is important to understand its strengths and limitations to see if it is the appropriate implementation of FROG to measure a given ultra-short laser pulse.

In this paper, we theoretically and experimentally examine the practical aspects of GRENOUILLE to aid its understanding and design. We discuss alignment, sensitivity, calibration, and bandwidth issues. We also give a procedure for the design of GRENOUILLE, useful in both the adaptation of existing GRENOUILLE devices, and in building new ones.

2 Wavelength range and tunability

While there is some use in designing a GRENOUILLE device for measurement of a given target pulse, it is even more useful to know how that device performs with pulses of different bandwidths, and even different wavelengths. As previously discussed, the SHG crystal's non-zero phase-matching bandwidth or, equivalently, its group-velocity mismatch (GVM) provides the spectral resolution of the device, and hence places a lower limit on the smallest spectral feature that can be accurately resolved, including the pulse bandwidth itself. For an SHG crystal of length L , and a pulse width of τ_p , this condition is

$$\text{GVM } L \gg \tau_p \quad (1)$$

or

$$A \text{ GVM } (\lambda_0) = \tau_p / L, \quad (2)$$

where the dependence of the GVM upon λ_0 is made explicit, and A is a 'safety factor', such that if A is much larger than 1, the relation is well satisfied. The case $A = 1$ is the 'ragged edge' of a given crystal, where the spectral resolution is on the order of the pulse bandwidth, similar to using a spectrometer to measure a line width equal to the spectrometer's resolution. Equation (1) is for GRENOUILLE only, where phase mismatch is the mechanism for spectral resolution. For normal SHG FROG, the converse is true ($\text{GVM } L \ll \tau_p$), to ensure that all wavelengths are phase matched simultaneously, requiring thin SHG crystals and resulting in much lower signal on each shot.

Similarly, the GVD places an upper limit on the pulse bandwidth, and the relevant relation is

$$\text{GVD } L \ll \tau_c, \quad (3)$$

as

$$\text{GVD } (\lambda_0) = A \tau_p / L, \quad (4)$$

where A again is the 'safety factor', and the coherence time τ_c has been replaced with the pulse length τ_p (assuming, for now, a near-transform limit). Here, the case $A = 1$ means the temporal spreading is on the order of the pulse, the temporal analogue of the $A = 1$ case for GVM. For normal SHG FROG, since GVM is kept small, and $\text{GVD} < \text{GVM}$ for all but single-cycle pulses, GVD is vanishingly small, and (3) is not even considered.

We can easily calculate the limits on the pulse bandwidth and/or transform-limited pulse width as a function of wavelength, by considering a given SHG crystal of length L , and choosing a safety factor A . Although measurements could be made for values of A near unity, a plot for various lengths of BBO with a conservative safety factor $A = 3$ is shown in Fig. 3a. The lower limit in the plots of minimum and maximum pulse lengths is the GVM equation, the upper limit is the GVD equation, and the shaded area in between is the area of safe operation, far from either limit. The point past which the lines cross is the point at which, for any bandwidth, the two conditions with $A = 3$ cannot be met simultaneously. Figure 3b shows analogous plots, but of the pulse spectral width and spectral resolution (minimum spectral structure) versus wavelength for the same parameters.

As the crystal thickness increases, the effective range of measurable pulses shifts to smaller bandwidths (larger pulse widths), as expected.

Just as spectrometers often operate at their resolution limits, it is also reasonable to operate a GRENOUILLE device for values of A near unity, that is, the limit of the device, as equipment specifications are usually presented, provided that the relevant deconvolutions are performed. Figure 4 compares the conservative case of $A = 3$ to the $A = 1$ case. The $A = 1$ case shows the wide applicability of a given SHG crystal in a GRENOUILLE device, so long as the limitations are well understood.

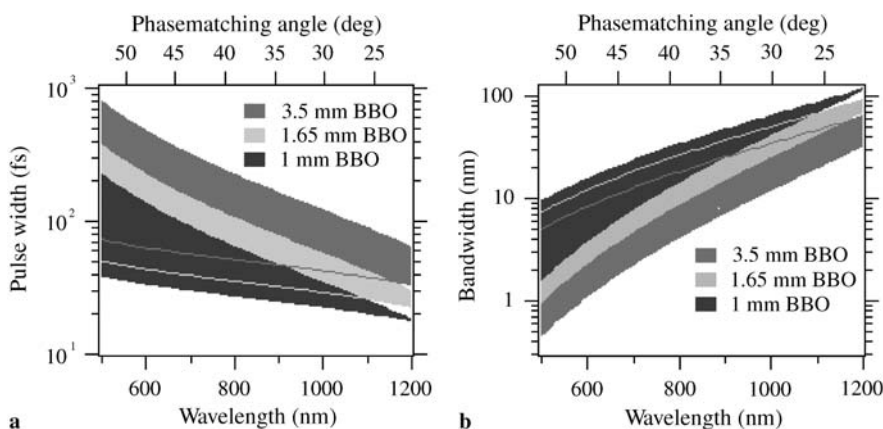


FIGURE 3 (a) With a reasonably conservative requirement on the GVD and GVM conditions ($A = 3$), there is still a good range of pulse widths that can be accurately measured with a given BBO crystal. (b) Same as (a), but plots are of the minimum and maximum bandwidths

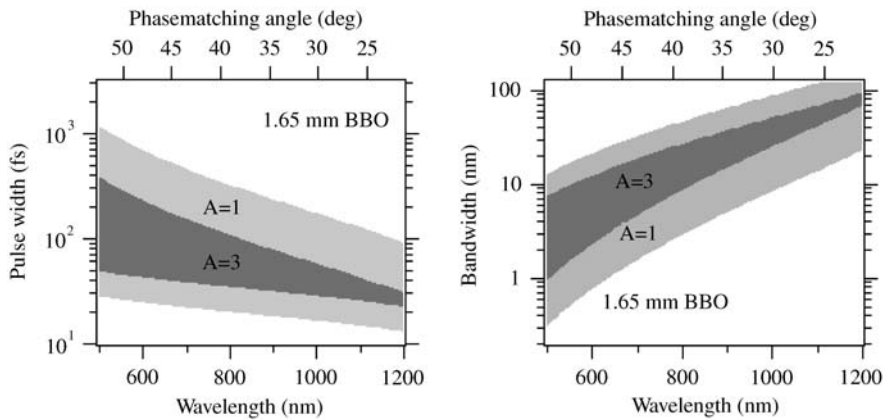


FIGURE 4 Pulse-width and bandwidth ranges for a GRENOUILLE device constructed of 1.65- and 3.5-mm BBO at two different safety factors A . The approximate phase-matching angles are shown at the *tops* of the plots

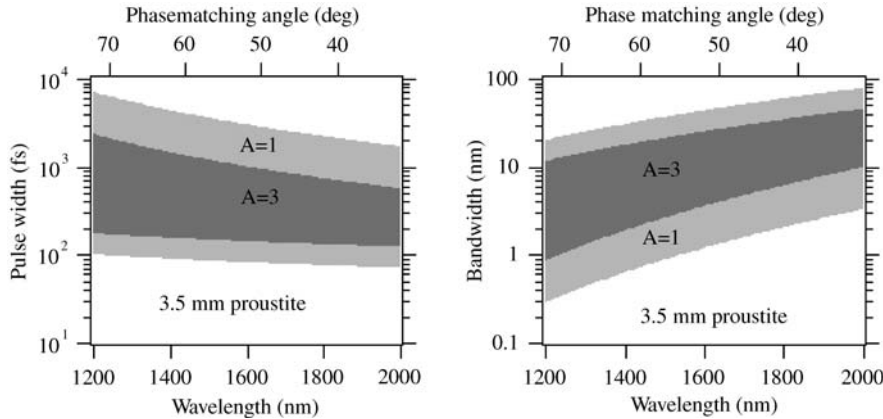
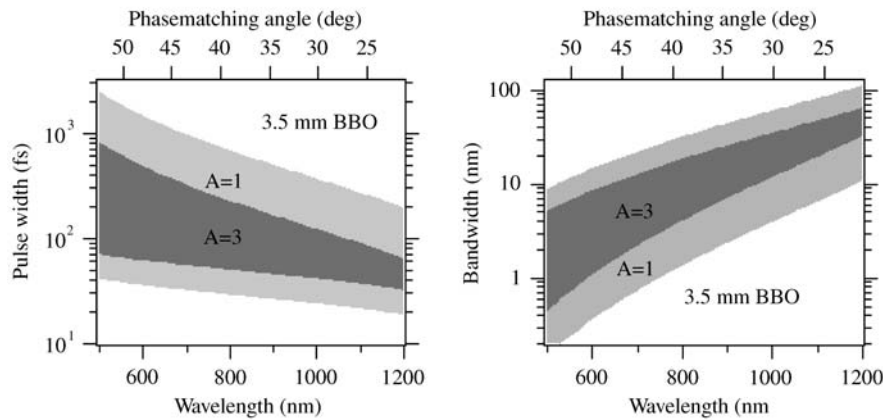


FIGURE 5 Pulse-width and bandwidth ranges for 3.5-mm of Proustite (AgAsS_3)

This type of plot is useful for finding crystals appropriate for other pulse-length, bandwidth, or wavelength ranges. One problem of great interest is relatively long pulses (~ 1 ps) at a wavelength of ~ 1.5 microns, but the SHG dispersion that GRENOUILLE requires is too low to design a GRENOUILLE device using most materials. Fortunately, we have found the obscure crystal, Proustite (AgAsS_3), to be an excellent candidate for such a GRENOUILLE device, even for quite narrow (1–2 nm)-bandwidth pulses (Fig. 5).

3 Design of a GRENOUILLE device

The design of a GRENOUILLE device is relatively straightforward. It begins by choosing an SHG crystal and estimating the required device spectral range. This corresponds

to a range of phase-matching angles in the crystal, which determines the beam divergence and confocal parameter, which should equal the crystal length. The crystal length, along with the pulse length, then allows a check of the device resolution and range using the plots or equations of Sect. 2. Finally, optics that yield the required beam divergence and delay range are easily chosen.

4 Experimental setup

For all of our experiments, except where noted, we used a Swamp Optics GRENOUILLE device with a compact folded geometry (Fig. 6). It includes a 12-mm iris at the input, a $\times 5$ beam-expanding telescope, a fused-silica Fresnel biprism with a 170° apex angle, a 150-mm focal length cylin-

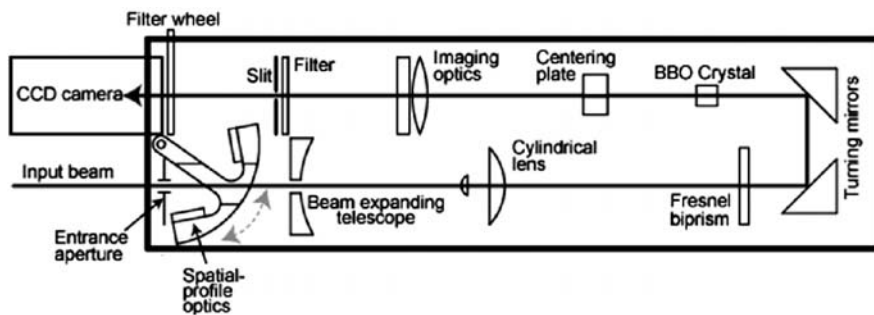


FIGURE 6 Compact, folded GRENOUILLE geometry. The spatial-profile optics (uncoated substrates) can be rotated into the beam for alignment and spatial profiling, or displaced out of the beam for pulse measurement

drical focusing lens, a 3.5-mm-thick BBO crystal and a back-to-back pair of 100-mm lenses, one cylindrical, one spherical. The lens pair creates an effective cylindrical focus of 50 mm in the delay direction, to perform one-to-one imaging in the usual $4f$ arrangement, and a 100-mm cylindrical focus in the wavelength direction, mapping crystal output angle to position on the camera, a Pulnix 10-bit 2/3"-format CCD camera. A BG-40 glass filter, placed just before the camera, passes the SHG FROG signal wavelengths but absorbs the input fundamental light. A slit, placed halfway between the BBO crystal and the camera, rejects the second-harmonic light generated by the two individual signal beams but passes the signal beam, which is focused to a line at this point. The beam is redirected halfway through the device with a pair of silvered prisms, to allow for the compact geometry.

Just inside the entrance to the device is a pair of uncoated substrates that can be positioned into the beam, in a preset fixed alignment, to send the beam directly into the CCD camera. The back surfaces of the substrates are roughened to eliminate any secondary reflections. While the CCD camera is much more sensitive to the 800-nm input light than the 400-nm second-harmonic light, only 1.6% of the 800-nm light is reflected into the camera when the substrates are in place. In this mode, the GRENOUILLE device functions instead as a beam profiler. The substrates are both aligned at 45-degree incidence angles, so that, when light is passing through the centers of the entrance iris and GRENOUILLE device optics, the beam is also centered on the CCD array. Aligning the beam into the GRENOUILLE device is accomplished very simply by centering the beam both on the entrance iris and the CCD image. These two points determine a line that ensures that the beam is aligned in x , y , θ and ϕ . Because the beam is easily observed at the input aperture and also on the camera output, it can be easily walked into alignment without the tedious alignment procedures required of other pulse-measurement devices, such as autocorrelators and interferometric methods. The substrates can then be switched to a 'closed' position, and the beam passes through the device correctly aligned, generating FROG traces directly onto the same camera.

Our laser pulse source was a KM Labs Ti:sapphire oscillator with a 90-MHz repetition rate, pumped by a Coherent Verdi (5.5 W). While capable of bandwidths ~ 100 nm, all the experiments listed here used pulses with ~ 30 -nm bandwidths.

To record the FROG traces, we used a Spiricon LBA-PC 200 frame-grabber card and associated software. Traces were typically recorded as 240×256 traces, but after binning the traces for retrieval, the traces, except where noted, were

64×64 . The trace binning and retrieval were performed using MATLAB FROG code that we have written, and pulse retrieval used the usual generalized projections algorithm [1].

5 Calibration

In a standard FROG device, which has a delay/beam-recombining arm and a spectrometer, calibration is a well-known procedure. The spectrometer can be calibrated using a standard calibration lamp with spectral lines at known wavelengths. For delay calibration in a multi-shot geometry (which uses a point focus in the crystal), one usually notes that each delay step on the translation stage corresponds to a known free-space difference in time, obtained by simply dividing by the speed of light. For instance, moving the delay stage in 1- μ m increments changes the path length by 2 microns (since it is a retro-reflector), corresponding to 6.67 fs of delay. In a single-shot geometry (which uses a line focus in the crystal), one of the delay arms is manually moved a known distance (and therefore a known time delay) and the shift, in pixels, of the FROG trace is recorded. Taking a series of traces at a series of known delays and computing a linear fit gives the temporal calibration in, say, fs/pixel.

It might seem that the innovations of GRENOUILLE make its calibration difficult, as there is neither an adjustable delay arm nor a spectrometer. But, in fact, its calibration is actually simpler. One method to calibrate the delay axis is to insert a material of known thickness and index of refraction immediately before or after either half of the biprism, creating a known delay which would then correspond to a shift of the trace in delay. To do this, its group delay must be known fairly accurately, and the thickness of the material must be sufficient to cause a discernable delay of one 'arm' versus the other, but not so thick as to cause considerable dispersion. These criteria are all attainable; for instance, the index of refraction of fused silica is known extremely accurately over a wide range of wavelengths, and a 1-mm chunk of fused silica induces a delay of 1.51 ps at 800 nm, while distorting a 30-nm bandwidth pulse from a transform limit of 31.3 fs to only 32.0 fs.

An even better method for calibrating the delay axis is to introduce a second trailing pulse with a known time delay after the original pulse. Building a Michelson interferometer, for instance, will create a single trailing pulse of adjustable delay. The resulting FROG trace has a center lobe and two side lobes, spaced apart from the center lobe by ΔT . The center lobe also has spectral fringes whose frequency spacing $\Delta\nu$ is the inverse of the temporal separation of the two pulses ΔT . Varying the delay of the interferometer varies not only

the distance between the side lobes and the center lobe, but also the spacing of the spectral fringes from coarse fringes at small delays to fine fringes at large delays. All three lobes will overlap at $\Delta T = 0$, and then one arm of the interferometer can be adjusted a known distance and, hence, time delay. Such a FROG trace will not only allow extraction of the temporal calibration, but also the frequency calibration, since the known time delay corresponds to a known fringe spacing $\Delta\nu$. Using the fringed spectral slice of the trace at $\tau = 0$, and the center wavelength of the trace (simply half the wavelength of the fundamental), one can easily extract the wavelength calibration.

Instead of creating a single trailing pulse, one can create a pulse train by using an etalon. This creates a FROG trace similar to the FROG trace of the double pulse, but which has a series of temporal side lobes, all of which have fringes. While the spacing is not variable, it can easily be inserted into the beam anywhere, making the calibration both portable and consistent. Furthermore, a linear fit can be made to the centers of all the lobes, giving a more accurate measure of the temporal calibration.

We calibrated our GRENOUILLE device using a 23.8- μm air-spaced etalon, which corresponds to a delay separation of 158.8 fs and a frequency separation of 6.30 THz (about 13 nm at a center wavelength of 800 nm). Fitting to the peaks of the delay and frequency marginals, we obtained a delay calibration of 2.17 fs/pixel and a wavelength calibration of 0.19 nm/pixel (Fig. 7).

While the reflectance of the interferometer beam splitter or etalon coating may have a somewhat limited wavelength range, the calibration can be made at one wavelength range and extrapolated to another. The delay calibration will not vary with center wavelength but, as the SHG crystal is tuned

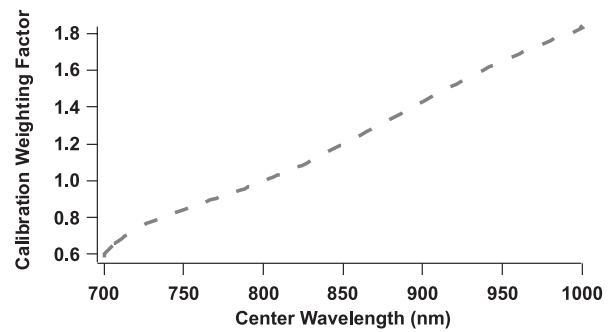


FIGURE 8 Theoretical scaling factor to adjust the spectral calibration as a function of center wavelength. Squares are experimentally measured calibrations, showing good agreement

to other wavelengths, the variation of phase-matching angle versus wavelength will change. However, this variation can be theoretically computed using the Sellmeier equations for the SHG crystal being used, or even for a new crystal to be swapped into the device. The derivative of this curve, computed numerically, gives the scaling factor to use as a function of tuned center wavelength. Using a tunable Coherent Mira Ti:sapphire laser, we confirmed our theoretical calculations for the calibration scaling at other wavelengths (Fig. 8).

6 Sensitivity

To measure the sensitivity of GRENOUILLE, we sent the oscillator pulse through a variable neutral-density filter with a graduated metallic reflective coating, and increased the attenuation, taking measurements of successively lower pulse energies. Using a variable-density filter instead of filter sets ensured the dispersion induced by the filter was equal for

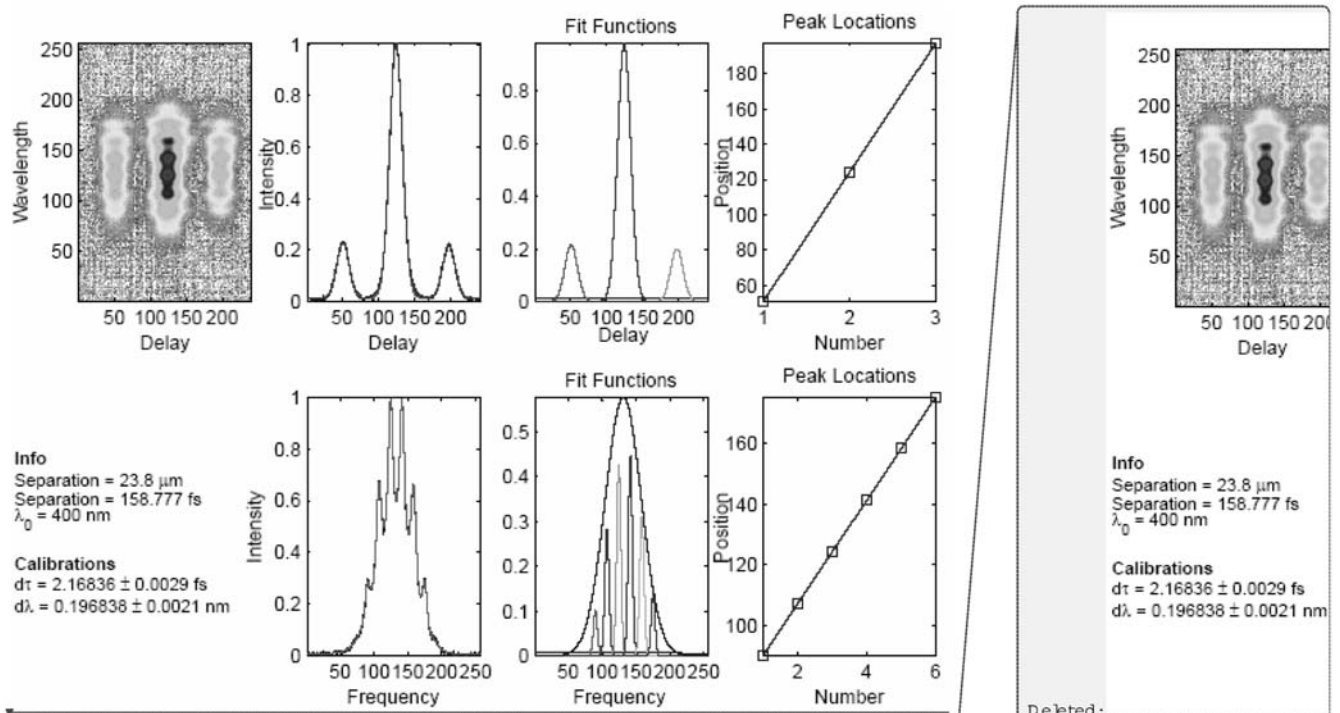


FIGURE 7 Etalon trace and a linear fit to peak locations extracts the calibration knowing only the etalon spacing and center wavelength

all measurements. We then ran the retrieval algorithm on each recorded FROG trace, and compared the retrieved intensities and phases.

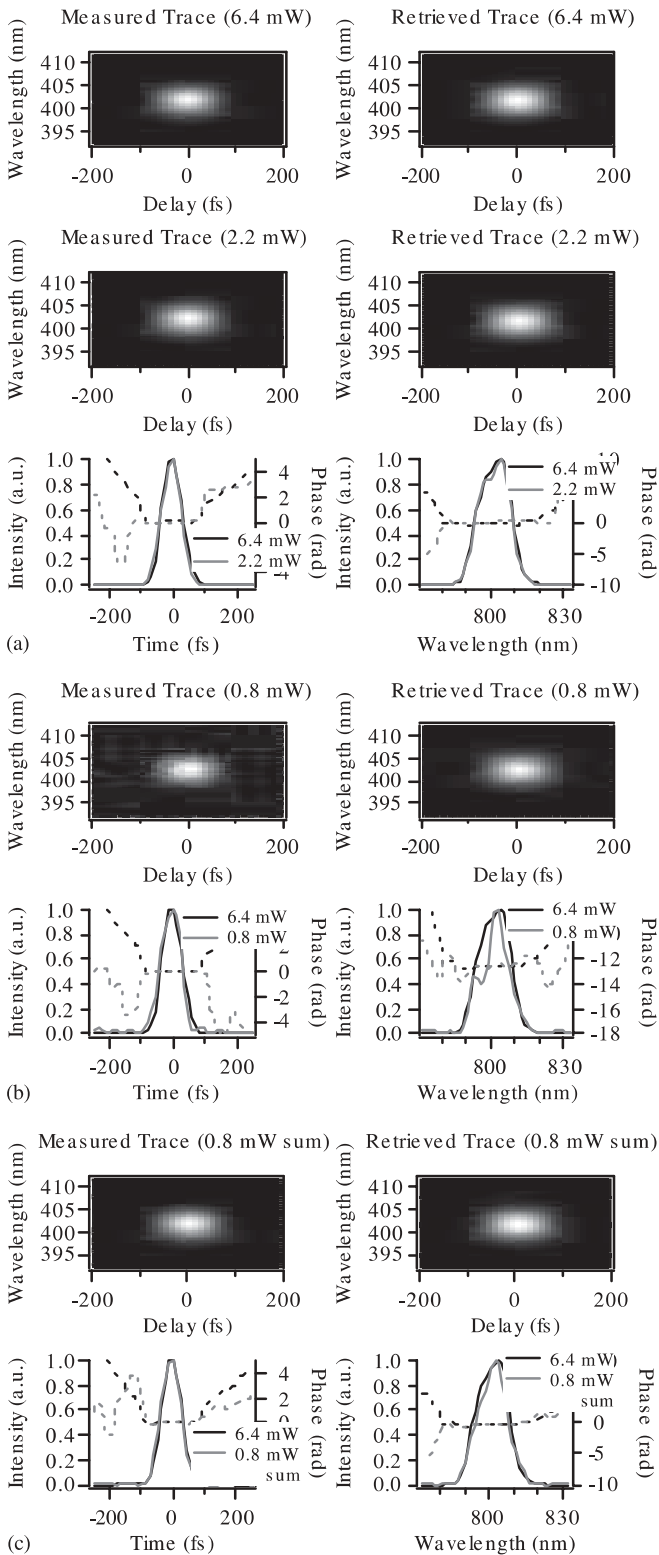


FIGURE 9 (a) Measured and retrieved traces, retrieved intensities and phases for 71-pJ and 24-pJ pulse energies, showing good agreement. (b) Comparison to 8.9-pJ pulses, where the signal to noise becomes too low. (c) Comparison to 64 summed frames of 8.9-pJ pulses, recreating good agreement

We made a reference measurement by adjusting the variable attenuator until the peak intensity of the FROG trace was just below saturation, at 6.4 mW or 71 pJ/pulse (Fig. 9a). Attenuating the power to 2.2 mW (24 pJ/pulse), the intensity and phase were still retrieved accurately (Fig. 9a). Around 0.8 mW (8.9 pJ/pulse) the signal-to-noise ratio became too low to measure an accurate FROG trace, and the retrieval became distorted (Fig. 9b). Employing frame summing on the Spiricon capture card (64 frames) increased the accuracy of the retrieval (Fig. 9c), but at the cost of much slower update rates (0.4 Hz or less), making the device impractical for real-time use.

Obviously, shorter pulses will have higher peak intensities, and stronger nonlinear signal strengths, and thus will be measurable by a given GRENOUILLE device at lower average powers. However, considerably shorter pulses will also usually require a slightly different GRENOUILLE beam geometry: one with tighter focusing (i.e. a larger divergence angle) to phase match the broader wavelength range, resulting in a shorter confocal parameter, and hence an effectively shorter crystal thickness, producing less nonlinear signal. The two effects approximately cancel. Thus, the exact minimum pulse energy that allows measurement of the pulse intensity and phase will vary only slightly, and 10 pJ/pulse is a good rough benchmark. The ability of GRENOUILLE to detect weak trailing pulses (those with a low contrast ratio) is about the same as in normal SHG FROG.

7 Spectral resolution

Since GRENOUILLE uses the narrow-band phase matching of a ‘thick’ SHG crystal to achieve its spectral resolution, it is important to measure the spectral resolution of GRENOUILLE. A reasonable estimate of the spectral resolution is provided by theoretically calculating the FWHM of the phase-matching bandwidth of a given crystal type and length. This is roughly equivalent to the smallest-scale features that can be discerned in the FROG trace. However, FROG is a joint time–frequency representation of the pulse, and so small-scale features in the spectral domain are easily represented as large-scale features in the time domain, even with poor temporal resolution. Therefore, a true test of GRENOUILLE’s spectral resolution involves not only the generation of the FROG trace, but the ability of the FROG algorithm to accurately retrieve the spectral structure, even ‘missing’ spectral structure, from the measured trace.

We built a simple Michelson interferometer to create a double pulse with a variable delay. The resulting FROG trace had a center lobe with spectral fringes, where the frequency spacing of the fringes $\Delta\nu$ is the inverse of the temporal separation of the two pulses ΔT , and two side lobes, spaced ΔT apart from the center lobe. Varying the delay of the interferometer varies the spacing of the spectral fringes from coarse fringes at small delays to fine fringes at large delays. We examined both the fringe contrast of the slice of the FROG trace at $\tau = 0$, and the retrieved pulse intensity and phase.

For small temporal separations (that is, small values of ΔT), the fringe contrast was very sharp, and the retrieved trace agreed well with the measured trace (Fig. 10a). As the separation is increased, the fringes became finer, but the re-

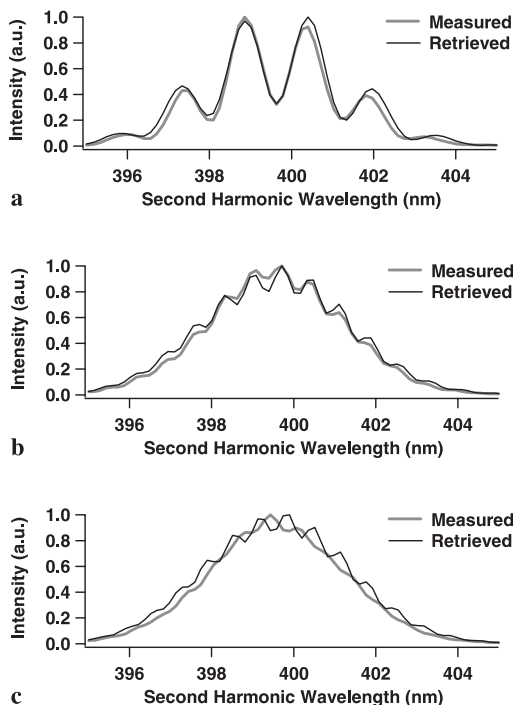


FIGURE 10 (a) Comparison of the measured and retrieved GRENOUILLE traces along the spectral slice at $\tau = 0$, for a pulse separation ΔT of 322 fs. The retrieved trace (FROG error 0.0001, 128×128 trace) reconstructs the fringes well. (b) Increasing the pulse separation to 726 fs still allows for reconstruction of the fringe spacing and location (FROG error 0.0068). (c) At $\Delta T = 806$ fs, the fringe spacing is still resolved by the temporal structure, but the fringe phase is no longer accurate (FROG error 0.0094)

tried location and contrast of the spectral fringes remained accurate (Fig. 10b). Even for pulses with significant separation and fine fringes with low contrast, the retrieved trace still accurately yielded the correct fringe spacing. When the fringes eventually do completely wash out, the FROG algorithm still retrieved the essential fringe structure, and the fringe spacing is correct, but the phase of the fringes became uncertain (Fig. 10c). GRENOUILLE is able to correctly retrieve the fringe spacing despite the lack of resolvable fringes because information in the delay direction is also available, which yields this information. However, determination of the spectral-fringe phase (and hence the relative phase of the pulses in the pulse train) requires the fringes themselves. The spectral resolution of our device corresponded to a pulse separation of about 725 fs, or a fringe spacing of 2.9 nm (at the fundamental wavelength, 800 nm), below which the fringe phase was indeterminate. Theoretically, the phase-matching bandwidth of the 3.5-mm BBO crystal we used was 1.4 nm (FWHM, at 800 nm), about half the experimentally determined minimum fringe separation of the device. This is similar to a spectrometer in ability, however, since measuring a spectral feature that is the size of the spectral resolution of the spectrometer will give an incorrect spectral width that is 1.5 to twice that of the feature being measured.

8 Sensitivity to input-beam misalignment

To test how robust GRENOUILLE is in the presence of input-beam misalignment, we aligned the device

using the spatial profiling optics and then rotated the device in fixed amounts, recording a series of FROG traces and comparing both the traces and the retrieved pulses to the perfectly aligned case. The GRENOUILLE device is compact and lightweight enough that it is easier to move the device by known amounts than it is to move or steer the beam. For both types of rotations, the GRENOUILLE device was rotated about an axis on the entrance iris.

8.1 Rotations about the crystal axis

If the GRENOUILLE device is rotated at the entrance pupil about an axis parallel to the crystal tuning axis, it simulates the beam entering the device at an angle non-collinear with the optical axis of the device. Instead, the beam appears to be entering 'up' or 'down' the frequency axis. Figure 11 shows the FROG trace of a pulse misaligned in one direction, i.e. tilted in the 'up' direction, and the retrievals of both directions compared to the correctly aligned retrieval, as a function of angle from the optical axis of the GRENOUILLE device. For angles of ± 3 and ± 6 mrad, there was a slight shift in the center frequency (as is the case in essentially all wavelength-measurement devices), but the retrieved pulse envelope and phase were relatively stable.

At ± 9 mrad, the distortion to the pulse envelope became more pronounced, and at ± 12 and ± 15 mrad the shape of the trace has clearly changed, and the retrieved spectrum has shifted by nearly half the spectral width. Thus, while GRENOUILLE, like essentially all other devices, yields a displaced spectrum when its input beam is misaligned in angle, it can accurately measure the pulse phase for misalignments of up to ~ 10 mrad, which corresponds to a considerable misalignment, more than two orders of magnitude more than that typically possible in, say, a spectral interferometry measurement.

8.2 Rotations normal to the crystal axis

For rotations about the other input axis (about an axis that is normal to the optical axis and the crystal tuning axis), the beam is entering the device to the 'left' or 'right', such that it enters the delay axis at an angle. However, when the delay axis is imaged onto the CCD camera by the $4f$ cylindrical lens system, the beams are initially focused to a point a distance f away from the CCD camera, with a slit placed there to filter out extraneous second-harmonic signal generated by the two individual beams (as made by the biprism). Any rays exiting the SHG crystal that are not parallel to the optical axis will be rejected by the slit. Thus, this walkoff quickly causes the signal rays to exit the crystal off-axis, and be clipped by the slit. Of course, the slit could easily be opened to account for this misalignment, but we have not done this, in order to simulate the performance of the actual device in practice. Figure 12a shows the pulse train generated by an etalon, with its corresponding (square-rooted) FROG trace and retrieved intensity and phase as a function of rotation angle. As the angle from the optical axis was increased (Fig. 12b and c), the signal level decreased and slight asymmetries occurred, but the FROG algorithm still accurately retrieved the intensity and phase from the trace. At an angle of about 9 mrad

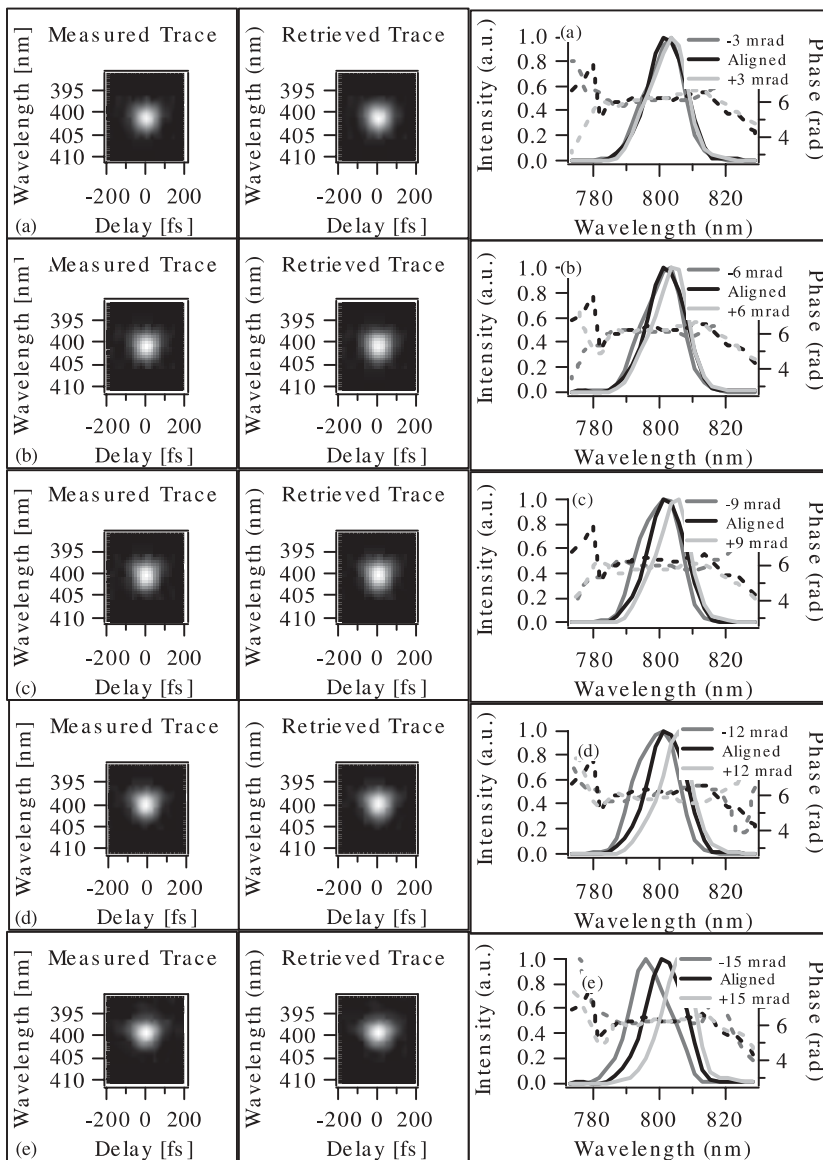


FIGURE 11 As the input beam is misaligned into the input iris about an axis parallel to the crystal tuning axis, the GRENOUILLE trace is shifted, and eventually distorts

(Fig. 12d), the signal was low enough and the trace asymmetric enough that the FROG algorithm converged incorrectly. (Only one direction of rotation is shown for clarity, but the results are qualitatively identical in the other direction.) It is interesting to note that the overall intensity drops off fairly evenly (the traces are rescaled to the peak), although there is some ‘directional’ clipping. This is because all the parallel rays, across the entire delay range, focus to a single line at the slit, and thus all the lobes in the trace are clipped at once. If instead a slit were closed down immediately after the crystal, we would see the outermost side lobes disappear first, and on in toward the center. No matter the length of the delay range across the crystal, the slit can, and should be, closed tightly about the exact line focus to eliminate spurious signal from the SH signal generated by each input beamlet.

9 Focusing issues within GRENOUILLE

Note that a transverse or longitudinal displacement of the biprism with respect to the SHG crystal has little to no

effect on the trace. As long as the beam has been expanded such that the beam profile is relatively constant across the biprism, the SH light that is the product of the intensities from each beam half remains the same. And as long as the biprism does not walk so far as to shorten the delay range covered by both beams to be less than the trace width, there is quite a bit of play with the biprism transverse or longitudinal location. To test the effects of biprism movement, we varied the crystal–biprism separation and found that it caused no discernable distortion to the FROG trace.

On the other hand, we found that the longitudinal position of the beam focus with respect to the crystal can yield distortions in the trace. This effect is not currently well understood, and we leave theoretical explanation for a later publication. We compared the measured FROG traces for various crystal positions with respect to the focal plane of the cylindrical lens. We first placed the crystal at the position which yielded maximum second-harmonic intensity (with the beam waist approximately at the center of the crystal) and, at that position, no distortions occurred. As the crystal was moved away from

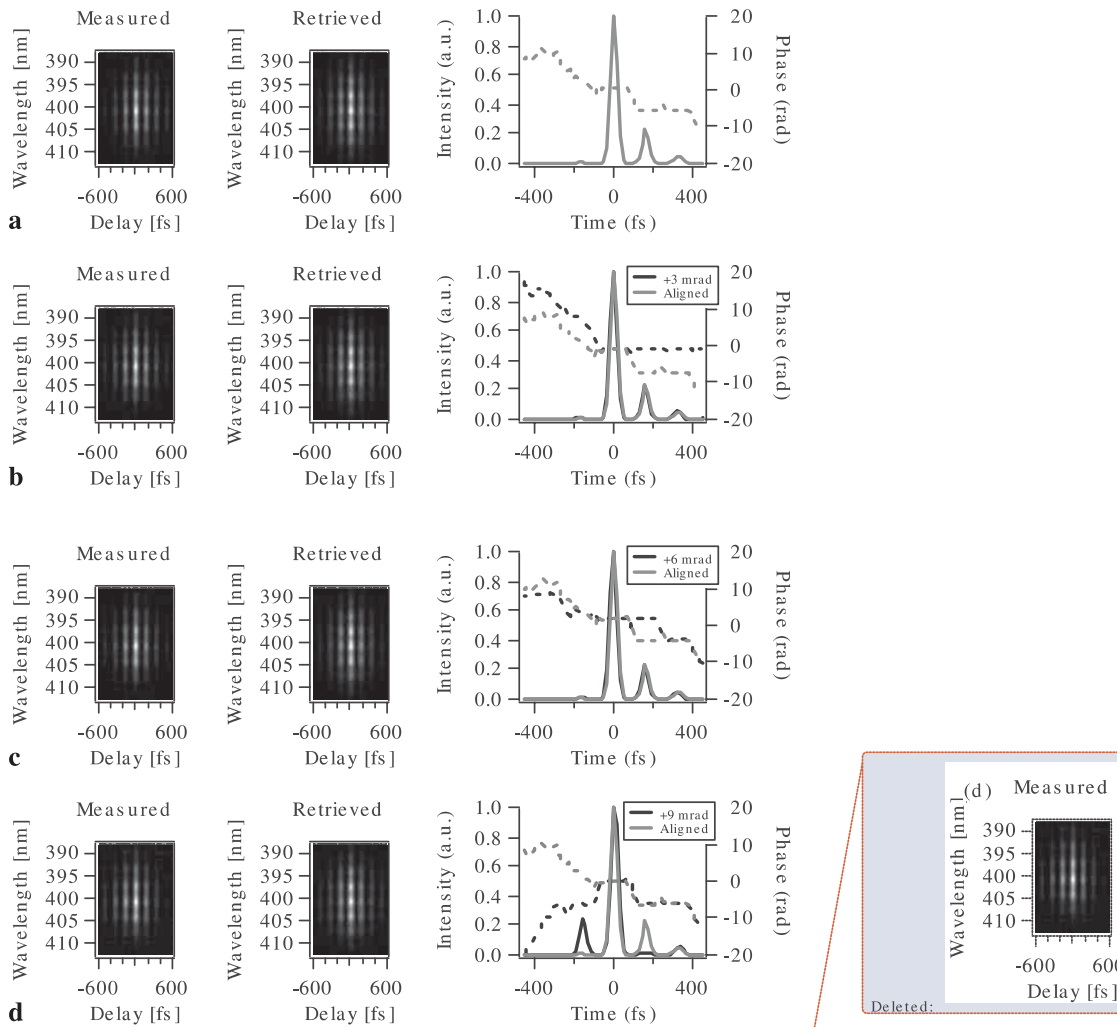


FIGURE 12 Effect of angular misalignment in the delay dimension. (a) Measured and retrieved GRENOUILLE traces of a well-aligned etalon pulse (square root taken for visibility). (b)–(d) As the slit begins to clip the signal beam, the trace distorts, and the algorithm eventually converges incorrectly

the cylindrical lens and the generated second harmonic became weaker, no distortions in the trace were observed. However, as the crystal was moved further toward the cylindrical lens (so that the beam focus occurred after the crystal), noticeable spatial distortions occurred in the generated second-harmonic beam. While the nature of the distortion is not fully understood, we find that it only occurs when the device is improperly aligned in this manner, and aligning the crystal for maximum second harmonic (and perhaps moving the crystal slightly away from the lens) easily avoids this distortion.

10 Conclusions

It is possible to build a GRENOUILLE device for a wide range of pulse-measurement applications. For designing, building, and aligning GRENOUILLE devices, however, the underlying constraints should be well understood. We

hope that our discussion and experiments have provided a set of useful procedures to follow to understand GRENOUILLE and its operation.

ACKNOWLEDGEMENTS This material is based upon work supported by the National Science Foundation under Grant No. ECS-9988706.

REFERENCES

- 1 D.J. Kane, R. Trebino: IEEE J. Quantum Electron. **QE-29**, 571 (1993)
- 2 D.J. Kane, R. Trebino: Opt. Lett. **18**, 823 (1993)
- 3 K.W. DeLong, R. Trebino, J. Hunter, W.E. White: J. Opt. Soc. Am. B **11**, 2206 (1994)
- 4 K.W. DeLong, R. Trebino: J. Opt. Soc. Am. A **11**, 2429 (1994)
- 5 D.N. Fittinghoff, K.W. DeLong, R. Trebino, C.L. Ladera: J. Opt. Soc. Am. B **12**, 1955 (1995)
- 6 P. O'Shea, M. Kimmel, X. Gu, R. Trebino: Opt. Lett. **26**, 932 (2001)
- 7 S. Akturk, M. Kimmel, P. O'Shea, R. Trebino: Opt. Express **11**, 68 (2003)
- 8 S. Akturk, M. Kimmel, P. O'Shea, R. Trebino: Opt. Express **11**, 491 (2003)